Int. J. Electrochem. Sci., 10 **(2015)** 9488 - 9512

International Journal of
ELECTROCHEMICAL
SCIENCE
www.electrochemsci.org

Review

Modern Development of Novel Electrode Materials as Effective Electrode Catalyst for Lithium Ion Batteries

Rasu Ramachandran[1], *Shen-Ming Chen*[2,*]

[1] Department of Chemistry, The Madura College, Vidya Nagar, Madurai – 625 011, Tamil Nadu, India.
[2] Electroanalysis and Bioelectrochemistry Lab, Department of Chemical Engineering and Biotechnology, National Taipei University of Technology, No.1, Section 3, Chung-Hsiao East Road, Taipei 106.Taiwan (ROC).
[*]E-mail: smchen78@ms15.hinet.net

Received: 27 June 2015 / *Accepted:* 11 September 2015 / *Published:* 30 September 2015

The most commonly used various electrode materials such as carbon fiber, multi-walled carbon nanotube, metal oxides, conducting polymers and nanocomposites for the improvement of electrode surface area, reduced the size, superior electrochemical performance and highly reversible cyclic stability in lithium ion batteries (LIB). Significantly, we have discussed about the analytical characterization techniques, morphological size (shape), choice of solvent electrolyte and temperature effects respectively. Furthermore, in order to discuss various electrochemical techniques like cyclic voltammetry, electrochemical impedance spectroscopy (EIS) and galvanostatic charge-discharge techniques have been used for testing electrochemical reactions and more in detailed studies of the reported discharged specific capacities and their reversible cyclic stability. The most important thing is previous and the recent reported novel based electrode materials of LIB studies for the execution of the future requirements of hybrid-vehicles and for electronic storage device applications.

Keywords: Anode, Cathode, Nanostructure, Porous structure, Ionic conductivity, lithium-ion battery.

1. INTRODUCTION

Recently, the most important requirement of energy storage devices (Fuel cells, super capacitors and batteries) for the operating of all the portable electronic devices, such as computers, hybrid vehicles, UPS, generators and invertors etc. In this type of power source based on the general principles, i.e. Conversion of chemical energy into electrical energy. Now a day, newly fabricated different kinds of electrode (Carbon fiber [1], multi-walled carbon nanotube [2, 3], metal oxides [4, 5], conducting polymers [6, 7] and nanocomposite [8, 9]) materials are using for boosting with high

energy density and larger power production rate. A novel nanostructured polycrystalline based $Li_{0.28}Co_{0.29}Ni_{0.20}Mo_{0.20}O_2$ thin film electrode exhibit good reversibility and high reversible specific capacity (216 mAh g^{-1}) in lithium-ion batteries (LIB) [10]. Kim *et al* [11] reported the silica nanoparticle-assisted-tuned cellulose nanofiber (S-CNP) electrode could possess a higher capacity (Around 130 mAh g^{-1}) and good cell performance in LIB. The unique porous structure and large specific surface area (~1066 ± 2 m^2 g^{-1}) of 3-dimensional graphene electrode material has been synthesized by hydrothermal and calcination methods. Here, calcinations play an important role in the formation of 3-dimensional porous morphology and it was displayed a reasonable reversible electrochemical performance [12]. Preparation of the nano flake porous structure of NiO/Ni electrode that are directly growing chemical liquid deposition method (CLD) under air atmospheric (350° C) conditions. The nanoporous materials showed their discharged and charged capacity value of 1.9 and 1.36 mAh cm^{-2} for 200 cycles [13]. Zhang *et al* [14] explored that the use of a facile rout for the synthesis of nanostructure ZnSe on reduced graphene oxide (rGO) nanocomposite, they founded that the significant synergetic interaction between ZnSe nanoparticle and rGO. The improved power performance had a reversible capacity value of about 876 mAh g^{-1} at mA g^{-1}. Nano sized $Ni_{3.5}Sn_4$ had a reversible capacity of 240 mAh g^{-1}, when it was used as the anode material for LIB. After the addition of carbon material, the kinetic parameter decreases and their reversible capacity value up to 273 mAh g^{-1} for more than 400 cycles [15]. Rohan *et al* [16] demonstrated that a novel functionalized polystyrene based lithium poly(4-styrene sulfonyl) (pheny sulfonyl) imide) (PSSPSI) ion conducting polymer gel electrolyte being applied widely using in the LIB. The conducting chain polymer electrolyte has been evaluated the lithium cation transfer number (0.87), average molecular weight (M_w = 105,343) and it's discharged capacity (149 mAh g^{-1}). The high temperature annealed (2400 - 2800° C) anthracite-based graphite has potential for an array of higher structural and crystal oriented catalyst illustrated their reported reversible high capacities (~250 mAh g^{-1}) [17]. The electrochemical properties of a wide variety of one-dimensional (1D) nano sized lithium iron phosphate ($LiFePO_4$) cathode and Co_3O_4-carbon nanotube based anode electrodes were exploited in energy storage devices by cyclic voltammetry and galvanostatic charge-discharge method. Especially, 1D nanostructured electrode showed excellent potential and good electrochemical properties in LIB [18]. Preparation of carbon particle-carbon sheet and iron oxide- carbon particle-carbon sheet (CP-CSs), (Fe_3O_4-CS-CNs) composite by Want *et al* [19] may effort have been made to combine carbon particle, iron oxide and carbon sheets to produce the superior discharged capacities. Recently, more efficient and highly active electrode materials and different kinds of electroanalytical techniques have been overviewed in various electrochemical fields, such as sensors [20], bio-sensors [21], pesticide sensors [22], solar cells [23] and supercapacitors [24] etc,.

In the present article, we have discussed that the different electrode materials, in specifically nanostructured morphological shape and sizes were widely used in LIB applications. Particularly, the authors are mainly focused on easily available materials, simple preparation, safety usage, cost-effective, environment friendly and good cyclic stability of energy storage devices. Therefore, in this review article making progress in the recent, fundamentals and scientific, reliable discussed LIB literatures for our younger researchers.

2. ELECTRODE CATALYSTS

2.1. Carbon catalyst

Germanium-carbon (Ge/C) based electrode catalyst for conducting 0D-in-1D morphology have been developed with the hope of improving the possibilities and new findings of lithium-ion energy storage devices. The as-prepared Ge/C nanowire exhibit high energy storage (1200 mA h g^{-1}) specific capacity with its excellent retention stability (500 cycles) for LIB [25]. The electro active nitrogen-doped carbon nanotube on graphene felt (N-CNT/GF) electrode has been explored extensively in battery performance. The porous structure of N-CNT/GF showed better enhancement of specific capacity and energy storage efficiency than CNT/GF as shown in Fig.1 [26].

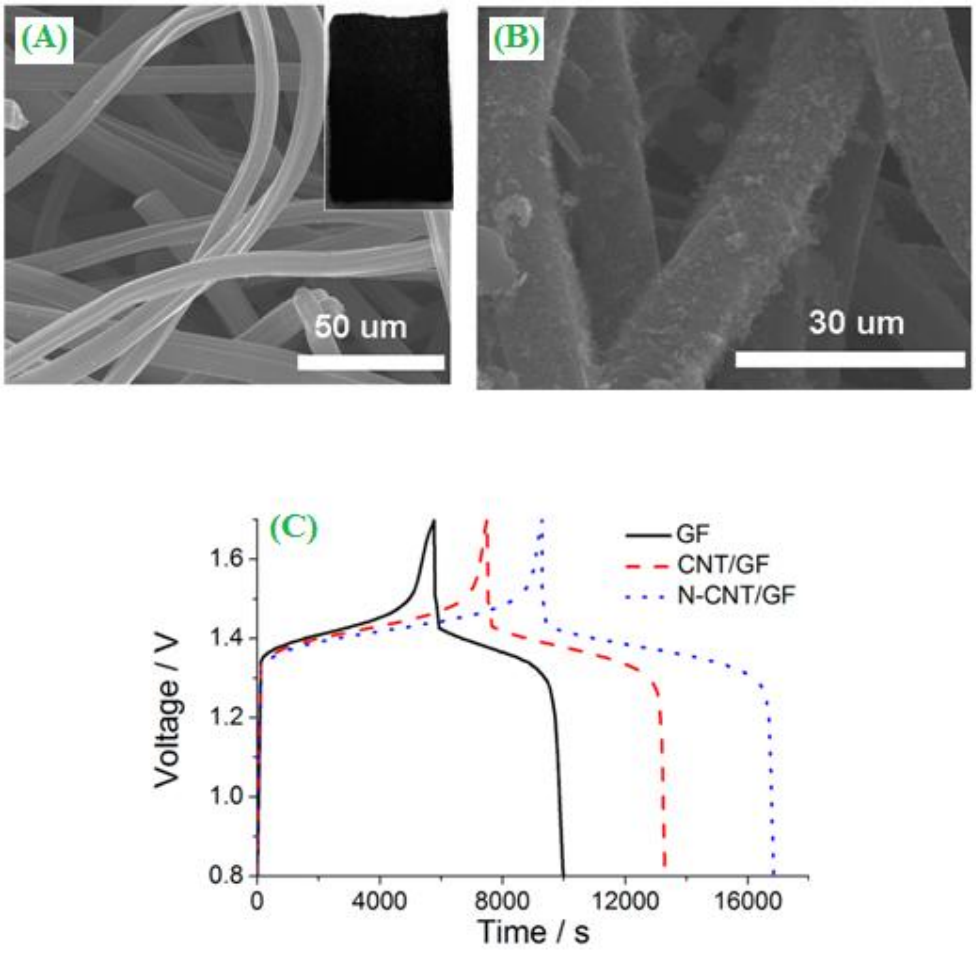

Figure 1. SEM images of (A) pristine GF with the inset showing the photograph of a typical GF (B) CNT grown on GF (C) Charge-discharge curves of the pristine GF (black), CNT/GF (red), and N-CNT/GF (blue) electrodes. ("Reprinted with permission from (*J. Phys. Chem. Lett. 3 (2012) 2164-2167*.). Copyright (*2012*) American Chemical Society").

A multi-constituent dual template method has been used for the preparation of three-dimensional ordered macro porous and mesoporous (3DOM/m) of $LiFePO_4$/C composite cathode, it can be significantly applied in LIB (2720 mA g^{-1}) [27]. A large scale CNT can be introduced into the

silicon (Si-CNT) by vapour deposition method. The fabricated ultra strong Si-CNT nonwoven performed better electrocatalytic activity (~494 mAh g^{-1}) and higher specific strength [28]. The highly electrochemically active nitrogen-doped graphene specific hollow spheres (NGHSs) have been synthesized by the template sacrificing method. The resulted electrode catalyst showed the discharge capacity value of 2716 mAh g^{-1}, which was higher value than that of theoretical graphite discharge capacity (372.0 mAh g^{-1}) value [29]. Wang *et al* [30] made a solvothermal method for the preparation of highly regulated peanut-like Fe_3O_4@N-rich carbon (Fe_3O_4@CN) microspheres. The result showed, a higher specific capacity (670 mAh g^{-1}) and excellent cyclic stability (30 cycles) than bare Fe_3O_4. The understanding of electrocatalytic capacity was an important parameter for the development of LIB ie, the enhanced reversibility of red phosphorous/activated carbon (P/AC) nano scale composite act as an anode electrode material [31]. The superior energy storage devices of free standing and bendable carbon nanotube/TiO_2 (CNT/ TiO_2) nanofiber nanocomposite has been synthesized by flow-direct assembled method [32]. A binder-free, current collector-free carbon nanofiber modified electrode spun polyacrylonitrile (PAN-CNFs) composite have been used as an anode electrode material for LIB studies by heat treatment temperature (800 and 1500° C) method [33]. The functionalized and mesoporous Co_3O_4/CNT nanocomposite has been mainly used in electrochemical (LIB) studies, especially the delivered high specific capacity value of 815 mAh g^{-1} [34].

2.2. Porous electrode

Ye *et al* [35] have reported that a systematic analysis and structural optimization of three dimensional nanoporous Au/TiO_2 core-shell electrode caused a greatly increased in both the power performance of supercapacitor and LIB.

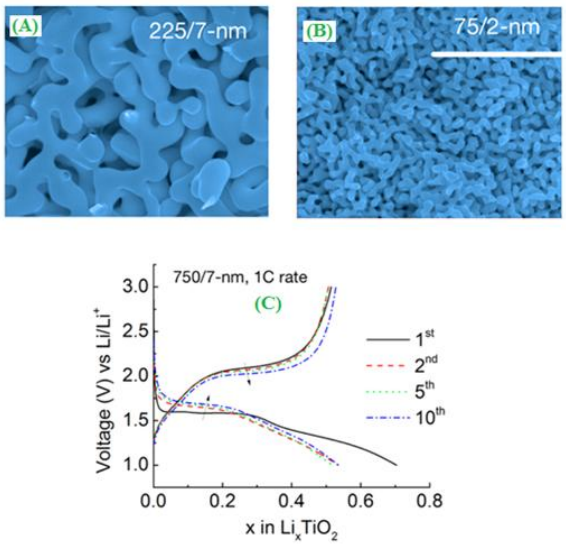

Figure 2. (A) & (B) Relevant transport processes and microstructure of 3D np-Au/TiO_2 electrodes for lithium ion batteries (C) Voltage profiles collected from 750/7-nm anatase samples during the first 10 cycles at 1C rate. ("Reprinted with permission from (*ACS Nano 9 (2015) 2194-2202.*). Copyright (*2015*) American Chemical Society").

Fig.2 Shows the SEM images of annealed (600° C for 1h) TiO_2 atomic layer deposition (ALD) coated nano porous Au coated on the electrode surface with three different nano pore sizes were obtained (75, 225 and 750 nm), the annealed 3D np-Au/TiO_2 core-shell electrode catalyst performed high reversible discharged capacity value of 236 mAh g^{-1}. The solvothermal (280° C) method prepared flower like porous hierarchical spherical morphology of Co_3O_4 electrodes were exhibited large BET surface area (72.5 mAh g^{-1}) and high discharged capacity (1316 mAh g^{-1}) value [36]. Electrochemical high power capacity was investigated as an infiltrating method of hierarchically porous monolithic $LiFePO_4$/C composite electrode and it was optimized calcined temperatures (650 to 800° C) for the investigation of lithium battery application [37]. Gowda *et al* [38] prepared three-dimensionally engineered porous silicon (Si) amorphous nanoparticles (10, 40 and 100 nm) embedded into Ni on the stainless steel electrode. This 3D nano film electrode showed better electrocatalytic (1650 mAh g^{-1}) activity, rate capability and superior cyclic stability. A simple method has been used for the preparation of porous and spongy like silicone powder etching Al-Si alloy powder. In this porous catalysts were characterized by BET (surface area of 102.8 m^2 g^{-1}), cyclic voltammetry and charge/discharge methods. Moreover, the inexpensive porous silicone based electrode contained the first cycle capacity value of 3450 mAh g^{-1} [39]. A three-dimensional (3D) porous C/$LiFePO_4$/MWCNT composite has also been proved to be suitable host cathode electrode materials for LIB's ultrahigh rated capacity, excellent discharge capacity (169.6 mAh g^{-1}) and good cyclic (200 cycles) stability [40]. A green and facile economical method was another viable approach in the fabrication of hollow porous MnO/C composite. This type of metal oxide based composite act as an attracted energy storage device due to their enhancement of electrochemical (700 mAh g^{-1} at 0.1A g^{-1}) properties, sustainable and green biocompatibility [41].

2.3. Nanostructured electrode

Recently, a novel procedure for the fabrication of nano sized $Li_4Ti_5O_{12}$/Carbon (N-LTO/C, 20-50 nm diameters) core-shell electrode has used most promising anode electrode materials for the next generation LIB. This kind of core-shell nanostructured electrode's applied potential value ~1.55 V and the reported discharged capacity value of 161 mAh g^{-1}. In addition that, the ionic and electronic resistance also been evaluated by EIS analysis (Fig.3) [42]. The tailored "one spot" method for the synthesis of tin-embedded carbon-silica (CS) nanostructured composites have been characterized by electrochemical method. The general observations were made from the reported Sn-CS composite showed an excellent reversible capacity and high columbic efficiency (67 %) [43]. The high performance conductive graphene nanoribbon and tin oxide (GNRs/SnO_2) nanocomposite has been shown to be about higher reversible capacity (1520 mAh g^{-1}) than that of theoretical reported capacity (372 mAh g^{-1}) value of graphite electrode [44]. The unique nanostructured and 3D tin oxide (SnO_2) catalyst, which can be attributed to enhanced the electrochemical performance and it was synthesized by chemical vapour deposition (CVD) method.

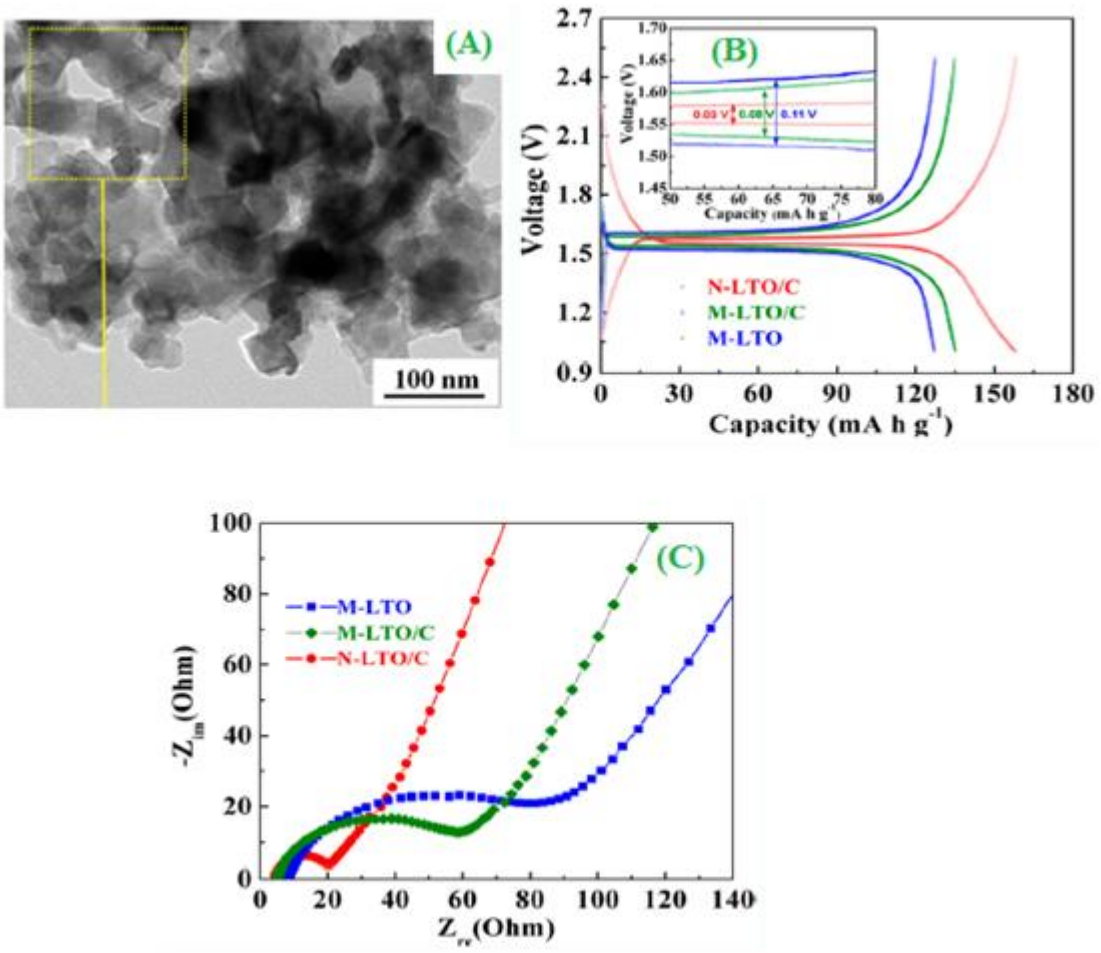

Figure 3. (A) Typical TEM images of the N-LTO/C core-shell nanocomposite (B) Electrochemical properties of the prepared N-LTO/C composite voltage profiles at 0.5 C (C) Nyquist plots of N-LTO/C, M-LTO/C, and M-LTO. ("Reprinted with permission from (*Nano Lett., 12 (2012) 5673-5678.*). Copyright (*2012*) American Chemical Society").

The as-prepared thin-film electrode plays an important role to optimize their specific capacity and long durability. The higher magnification SEM image of columnar nanostructured SnO_2 grain size is about less than that of 20 nm, the reversible capacity value of 352.8 μAh cm^{-2} μm^{-1} [45]. Nanolumanar morphology of silicone thin film electrode extended the onset of low temperature annealing for the significance of reversible capacity and excellent cyclic stability in lithium ion battery analysis [46]. Among them, antimony/carbon (Sb/C) composite has been widely studied for the electrochemical impedance spectroscopy of LIB. The main electrochemical observations, 50.1 % Sb/C (Annealed at 400° C) (Sb_5) composite showed superior charge transfer resistance value than Sb_4 and Sb_6 [47]. Alfaraqui *et al* [48] have used one step polyol assisted pyro-synthesis method for the preparation of nanostructured spinal $ZnMnO_4$/C composite, the measured spherical particle size range of 10-30 nm. This composite electrode tends to improve their delivered high capacity value of 666.1 mAh g^{-1} and good cyclic stability (50 cycles).

2.4. Conducting polymer

The initial attempts were actually made for improving the possibilities of covered poly(3,4-ethylenedioxythiophene) (PEDOT) on a non-stoichiometries Li-rich manganese oxide electrode by the sol-gel method. The main objectives, negative graphite and positive MnO_2/PEDOT electrodes were exhibited better electrochemical (battery) performance [49]. Sharma *et al* [50] reported perylene-3,4,9,10-tetracarboxylic dianhydride (PTCDA) polymer electrode was made better re-chargeable lithium storage battery applications. The needle-like morphological electrode showed their improved electrochemical performance was confirmed by EIS technique (Fig.4).

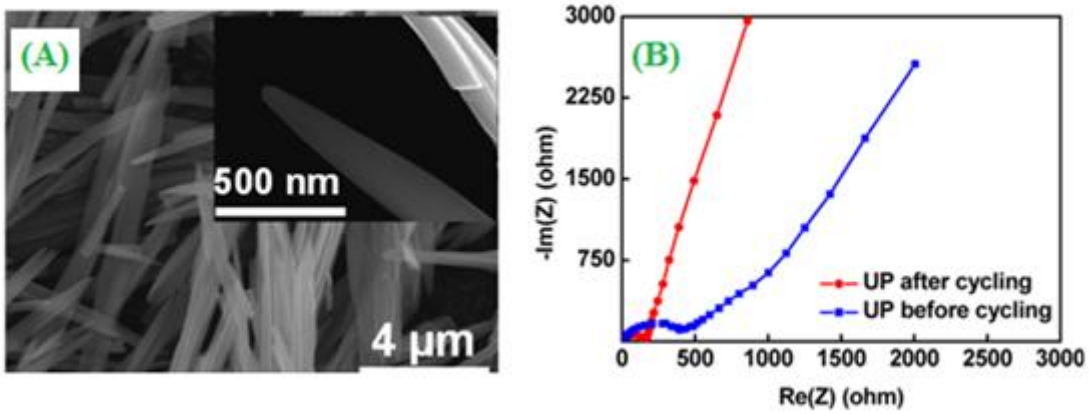

Figure 4. SEM micrographs of PTCDA and polyimide derivatives (A) HP shows needle-like morphology (B) Electrochemical impedance spectra of UP recorded before cycling and after 100 cycles of charge discharge at 200 mAg^{-1} for each of the samples. ("Reprinted with permission from (*J. Phys. Chem. Lett., 4 (2013) 3192-3197*). Copyright (*2013*) American Chemical Society").

Pyrolysis rout method using a polymer (Polysilane-HTT1800)-derived SiCN ceramic composite provided novel electrochemical applications. The anode composite material was characterized by Raman analysis, the highly distorted carbon composite's well-pronounced D-band at 1347 cm^{-1} and the exhibited recovered capacity value of 434 mAh g^{-1} [51]. Liu *et al* [52] used two different polymers (Polyorganosilazane-HTT1800 and polyorganosilaxane RD-684a) modified with divinyl benzene (DVB) composite act as a negative electrode. In addition to that the free carbon corresponding of SiCN and SiOC ceramics. The higher carbon content-polymer derived composite negative electrode obtained the highest storage capacity value of 574 mAh g^{-1} and the columbic efficiency was raised up to 10 to 60.4 %. The most development of single ion conducting polymer electrolyte membranes was used in different molar ratios (2.0/1.5), especially polyvinyl alcohol with boric acid, oxalic acid and lithium carbonate. However, the uptake of lithium polyvinyl alcohol oxalate borate (LiPVAOB) molar ratios of single-ion conducting polymer membrane electrode exhibited high ion conductivity for lithium ion battery applications [53]. A new approach involving the polymer electrolyte of polymeric lithium tartaric acid borate (PLTB) has been synthesized by one-step processes. This electrolyte membrane was modified with poly(vinyldine fluoride-co-hexafluoro

propane) (PVDF-HFP) using a doctor-blading method. This was soaked with propylene carbonate (PC), the optimized (Annealed 80° C) PC swollen PLTB@PVDF-HFP composite exhibit high ionic conductivity and excellent promising application in electrochemical stability [54].

3. STRUCTURAL AND MORPHOLOGICAL CHARACTERIZATION

Wang *et al* [55] prepared a turbostratic carbon nanosphere (CNSs-2) by ultrasonic polymerization (Polypyrrole nanospheres (PNS-2)) method. The analytical studies of X-ray diffraction (XRD) were used as a versatile technique for the optimization of the assigned (PNS-2 and CNS-2) 2θ peaks at 25 and 43° and their corresponding reported (002) and (101) plane. In this pattern, PNS-2 exhibit weak and broad peaks (25.2°) due to clearly indicate the amorphous nature of the polymer sample. Electrospining method has been used for the preparation of non-woven poly(acrylonitrile) (PAN) fibrous membrane act as a polymer electrolyte in LIB studies. The chemical structure of the PAN-4 membrane, the before and after electrospinning of two identical spectral peak (−C≡N at 2243 cm^{-1}) was observed from FT-IR spectrum [56]. Similarly, the electro active phase-pure Cu_4O_3 microspheres have been prepared via solvothermal method.

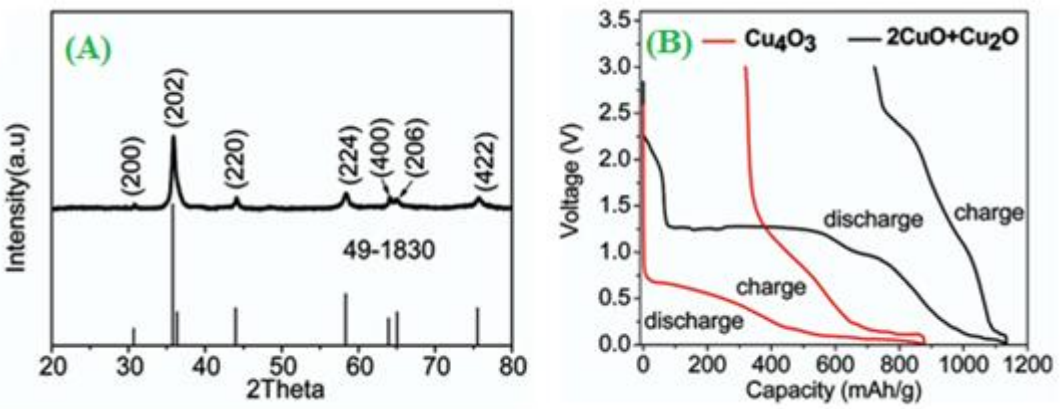

Figure 5. (A) XRD pattern of Cu_4O_3 microspheres (B) Electrochemical properties of Cu_4O_3 and the 2CuO + Cu_2O composite: Initial discharge and charge curves (0.0-3.0 V and 0.1 C). ("Reprinted with permission from (*Chem. Mater 24 (2012) 1136-1142*). Copyright (*2012*) American Chemical Society").

Fig.5(A), the XRD pattern of copper oxide also exhibits different diffraction peaks at 30.7°, 35.8°, 44.0°, 63.9°, 65.0° and 75.0° were identified with their subsequent lattice plane of (200), (202), (220), (400), (206) and (422), which were clearly matched with the reported JCPDS (49-1830) values. However, the above synthesized Cu_4O_3 were highly pure and evaluated by electrochemical method (Fig.5(B)) [57]. In order to improve the carbonate based electrolyte has been reported for the best electrochemical performance at 253 K. The chemical structures of trifluoro ethylbutrate, ethylene trifluoro acetate, trifluoro ethyl acetate and methyl pentafluoro opropionate have been studied by FT-IR spectrum. The wave region of 3000-2815 cm^{-1} (C−H bond stretching), strong, sharp absorption

peak at 1790-1740 cm^{-1} (C=O stretching) and the sharp absorption at 1200-1050 cm^{-1} (stretching vibration in C−O−C ester group) [58]. Zahmatkesh *et al* [59] used a binary solvent ethylene glycol to play an important role in the hydrothermal assisted synthesis and characterization of bow-tie-like lithium ion phosphate ($LiFePO_4$) nanocrystal, which was improved the performance of electronic and ionic conductivity (166 mu g^{-1}) of LIBs. In recent years, the mono dispersed nano cages of CoS_2 can be modified with graphene nano sheets (CoS_2/G) composite signify a new mode for the improving of electrochemical performance. The composite has been characterized by XRD, Raman spectrum and thermogravimetry analysis (TGA). Whereas, the microstructure CoS_2/G composite could effective matrix and the nano cage structure could enhance the capacity (800 mAh g^{-1}) and good cyclic stability (300 cycles) of the anode catalyst [60].

The category of multi-valence transition metal ions into metal oxide electrodes have been evaluated by morphological and achieved their higher discharge capacity studies. The most 3D morphological structure of Ni ions was distributed uneven and its single LNMO particles of Mn and Ni were projected at different angles. Ni surface modification methods are mainly dependent on temperature and growth time.

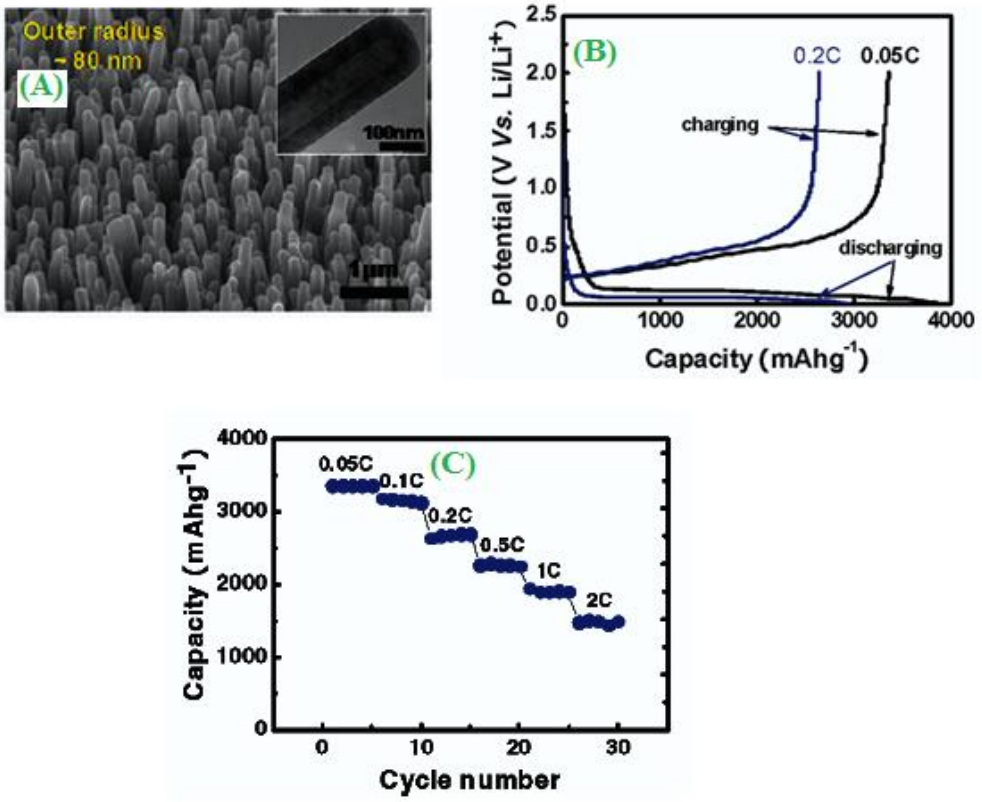

Figure 6. (A) Electron microscope images and elemental line profile analysis of Si NTs. SEM image of a vertically aligned Si NT array with R_{out} ~ 80 nm (B) Electrochemical characteristics of the Si NT array electrode (R_{in} ~ 30 nm and R_{out} ~ 60 nm), Voltage profiles for the first cycle at a rate of 0.05 and 0.2 C. (C) Rate capabilities of Si NT array electrodes at various C rates. ("Reprinted with permission from (*Nano Lett., 10 (2010) 1710-1716*). Copyright (*2010*) American Chemical Society").

This type of Ni selective surface can impact the general approach and tailoring electrode surface for the improvement of discharge capacity and its higher power rate [61]. Hybrid nano fiber of polyaniline/polyoxomatalate (PANI/PMo_{12}) composite has been synthesized by interfacial polymerization method. It was characterized by SEM and EDX analysis. This result was clearly explained the nanofiber diameter of 100 nm and the EXD spectroscopy, which was confirmed by the incorporation matrix of PANI/PMo_{12}. This type of nanofiber matrix was delivered a remarkable improved discharged capacity value (183.4 mAh g^{-1}) [62]. In general, a novel amphiphilic conductive polynorborane modified with the pendent cyclotriphosphazene material play an important role in the performance of lithium-ion sea water batteries. The substituted structure of polymer utilized side chain groups able to give a higher density of functional side chain units [63]. The use of nanostructured arrays of sealed silicon anode as active electrode materials in energy storage devices. Fig.6.A. Shows the SEM images outer radius of around ~80 nm and elemental analysis of silicone arrays nanotube (Si NTs). Similarly, (Fig.6.B&C) the electrochemical performance and rate capability of Si NTs exhibited the charging and discharging capacitive values like 3860 ± 20 and 3360 ± 20 mAh g^{-1} respectively [64]. Fabrication of mesoporous lithium manganese silicate (Li_2MnSiO_4) has attracted considerable large surface area and shorter ion diffusion pathway for the potential application in LIBs. The XRD pattern of Li_2MnSiO_4 exhibit strong peaks at 2°-3° and the calculated diameter particle size value of 4.033 nm (Braggs Law). On the other hand, FT-IR spectrum also confirmed by the internal vibration of the silicate anion peaks exhibited in their particular positions like 890, 926 and 530 cm^{-1} [65]. Wu *et al* [66] have reported a bimetallic design and versatile technique for the preparation of ultrathin spinal membrane encapsulated layered lithium-rich electrode material in high power (290 mAh g^{-1}) electrochemical applications.

4. EFFECT OF PHYSICO-CHEMICAL CONDITIONS

4.1. Electrolytes

Chen *et al* [67] used ionic host solid electrolyte interface (SEI) on reduced graphene oxide electrode. A binary electrolyte of maleimide and water (MI/H_2O) additive, which were enhanced the reaction rate, reverse capacity and frequent potency of lithium ion batteries. The use of all-solid state lithium ion batteries (ASLBs) has been used as an alternative conventional energy storage device. However, the bendable and thin sulphide solid electrolyte films unbreakable with instinctively complaint nonwoven (NW) scaffold for free standing ASLBs [68]. The most novel electrolyte mixture of lithium hexafluoro arsenate ($LiAsF_6$) could be used directly in the next generation battery application. This was hastily development of the next generation electrolyte salt illustrated fast degradation under the electron beam source with higher electrochemical activities [69]. The consisted gel-polymer electrolyte (polyvinylidenefluoride-co-hexafluoropropylene (P(Vdf-HFP), 1-butyl-4-methyl pyridinium bis(trifluoromethane sulfonyl) imide) (B_4MePyTFSI)) and ionic liquid have been prepared by solution casting method. The gel-type polymer electrolyte ionic conductivity value of 2.01 x 10^{-4} S cm^{-1} at room temperature and it can be used an excellent supporting electrolyte for the study of high performance electrochemical reaction in rechargeable lithium batteries [70]. Zeng *et al* [71] used dimethyl phosphonate (DMMP) as a non flammable electrolyte solvent. $LiFePO_4$ and SiO (SiFe and

Sb alloy) act as a cathode and anode electrolyte for safety high power, large scale lithium ion batteries. This kind of phosphate electrolyte displayed great scope and large scale advantages in grid-scale energy devices. Very recently, the capacity of the glass-microfiber nonwoven supported cyanoethyl-β-polyvinyl alcohol composite electrolyte membrane (GFMFPE), which can be used as an heat resistance and rigid flexible supporting electrolyte explored high-performance electrochemical properties and enhanced mechanical properties of LIBs[72].

4.2. Effect of temperature

Today, new development of co-solvent used and wide range of temperature based LIBs. Particularly, 2,2,2-trifluoro ethyl N-carproat (TFENH) act as an electrolyte, X-ray photoelectron spectroscopy (XPS) and electrochemical techniques have been demonstrated that the thin and stable $CH_3(CH_2)_4COOLi$ film decomposed by TFENH deposition on the graphite electrode surface. Here, low temperature plays a crucial, performance and cyclic stability of lithium ion batteries [73]. Zhu *et al* [74] have discussed the electric vehicle (EV) and hybrid electric vehicle (HEV) by electrochemical impedance spectroscopy (EIS) method. By this EIS analysis, phase shift, the magnitude of impedance and the optimized inner temperature can be accomplished with battery management system. The standard liquid electrolyte of polydimethylsiloxane (PDMS) based grafted and ungrafted co-polymers (Poly[dimethyl siloxane-co-(siloxane-g-acrylate)] (PDMS-A), poly(dimethylsiloxane-co-phenylsiloxane)) have been used as a suitable additives of low temperature assisted electrochemical performance (discharged capacitive) and high rate capacity of LIB [75]. Carbon electrode can be modified with graphite flakes 80 wt %, 10 wt % of acetylene black and other 10 wt % of polyvinylinedine fluoride. The well dispersed materials have been coated on copper foil electrode and it dried at 110° C under vacuum conditions. The carbon-chain electrode was tested using electro analytical techniques; charge/discharge performance (Room temperature) and the largest capacity shrink LIB performed under low (245° C) temperature conditions [76]. Alternatively, nitrogen-treated hierarchical macro/mesoporous TiO_2 electrode was annealed under nitrogen and air conditions at 300° C (3h). In this anode electrode elevated at 55° C, significantly the improvement of considerable high capacity (293 mAh g^{-1}) and excellent performance in LIH [77]. Existing, the in situ temperature was extensively studied flexible polymer embedded thermocouple (TFTCs) monitored for the improvement of safety and high performance of LIB. The inside pouch cell heat generation battery, which dominant of the highest rate capacity [78]. The active electrode materials (Lithium cobalt oxide/lithium manganese cobalt oxide composite act as cathode and silicon/graphite composite act as an anode) and a bi-functional conductive additive (Lithium difluoro(oxalato) borate) have been used for the manufactured of performance-voltage in conventional energy storage (LIB) devices [79].

5. NITROGEN ADSORPTION-DESORPTION

The greatly enhanced electrochemical performance of phosphorous and nitrogen dual doped porous graphene (PNG) anode by MgO-template CVD technique. The BET specific surface area and

the porosity of the size distribution (2-10 nm) of PNG was used by N_2 adsorption-desorption, the reported specific surface area (SSAs) value of 1752 m^2 g^{-1} [80]. The simple *in situ* and electrospinning methods have been used for the fabrication of Fe_3O_4/C micro belts (FCBs). The surface morphology of micro belt with ~4 μm FCBs exhibited superior electrochemical (710 mAh g^{-1}) behaviour and N_2 adsorption-desorption studies SSAs value of 21 m^2 g^{-1} [81]. For instance, the novel Mn^{2+}-doped TiO_2 nanosheet-based spheres presents better electrochemical performance in LIB by hydrothermal and ion-exchange method. The N_2 adsorption-desorption studies of different calcinated samples (TiO_2-HT, HT-400 and HT-Mn-400) were estimated the typical different surface area values such as 110.7, 230.7 and 222.0 m^2 g^{-1} respectively [82]. In order to study the two different morphological structures of cocoon and rod shaped mesoporous iron oxalate (FeC_2O_4) electrodes have been extensively explored for the improvement of electrochemical conductivity and long durability of LIB. The SSAs of gas adsorbed A-Fe-O_x-R and A-Fe-O_x-C electrodes were exhibited 37 and 22 cm^3 g^{-1}, respectively. The prepared anhydrous FeC_2O_4 cocoons and rods like based electrodes showed their discharged capacity values of 1288 and 1326 mAh g^{-1} [83]. The mesoporous of Au/$Li_4Ti_5O_{12}$ spheres, which was widely used as the commercial electrode materials in LIB, the electrode noticeable good electrochemical performance. The pore size (2 to 5 nm) distribution has been calculated by Barrett-Joyner-Halenda (BJH) method and the studies SSAs value of 166 m^2 g^{-1} (Fig.7) [84]. The expected electrochemical synergetic effect of zinc oxide-loaded/porous carbon (ZnO-Loaded/PC) composite has been motivating factor in LIB, exploiting the good discharged capacity (653.7 mAh g^{-1}), large SSAs (319.11 m^2 g^{-1}) and tremendous cyclic stability (1000 cycles).

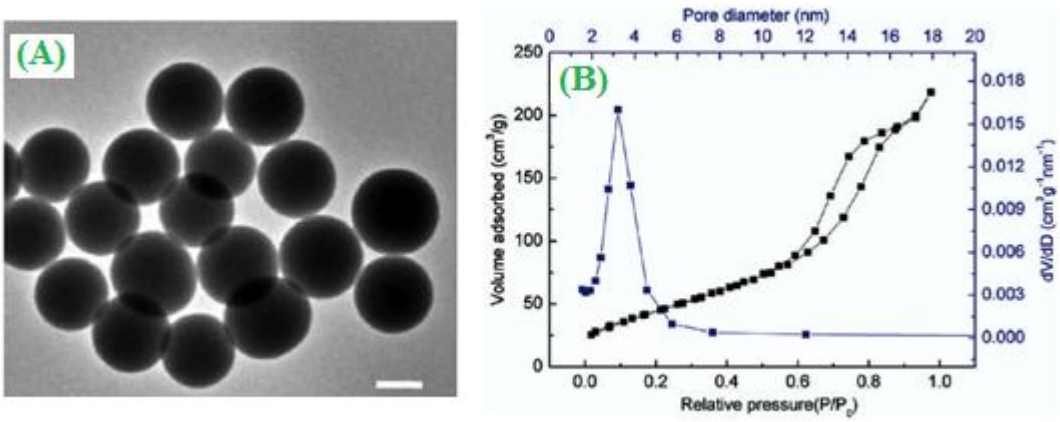

Figure 7. (A) Representative TEM images of titanium glycolate spheres prepared at low TBT concentration 0.8 mL of TBT in 50 mL of EG (B) N_2 adsorption-desorption BET isotherm and pore size distribution curve. ("Reprinted with permission from (*ACS Appl. Mater. Interfaces 4 (2012) 1233-1238*). Copyright (*2012*) American Chemical Society").

The rate of modified electrode to promote the intercalation/deintercalation of lithium ion electron transfer for the electrolysis [85]. On the other hand, graphene-encapsulated hollow Fe_3O_4 aggregate nanoparticle anode electrode material present better unvarying specific capacity and employed the estimated graphene encapsulated anode electrode surface (132 m^2 g^{-1}) used N_2 adsorption-desorption isotherm method [86].

6. ELECTROCHEMICAL STUDIES

6.1. Redox behaviour

Cyclic voltammogram is one of the most powerful electro analytical technique for the study of both oxidation and reduction species. Iron-manganese pyrophosphate (Li_2Mn_{1-y} $Fe_yP_2O_7$) has been founded a promising cathode material in LIB. The (+2) oxidation state of both Mn and Fe have been confirmed by thermo gravimetric and magnetic susceptibility methods. The reversible second oxidation peaks were observed at ~5 V for $Li_2FeP_2O_7$ and $Li_2MnP_2O_7$ for ~5.3 V, similarly Fe^{3+}/Fe^{4+} and Mn^{3+}/Mn^{4+} redox couples were electrochemically active [87]. A novel divalent iron nitridophosphate ($Na_2Fe_2P_3O_9N$) described a promising design strategy for finding new isolated ($[PO_3N]^{4-}/P[O_2N_2]^{5-}$) cathode tetrahedral building block material can be used as the next-generation phosphate based battery. The Cv curves were exhibited into two redox peak potential at 3.55 V/3.5 V and 3.1 V/2.95 V, these kind of redox peak potentials were clearly indicated that the PO_3N group [88]. Zheng *et al* [89] developed new innovative (*In situ* lithiation strategy) methods for the fabrication of a highly stable sprinkled sphere shaped sulphur/microporous carbon (S/MC) composite (Fig.8A). A simple electrochemical (CV) technique, which was used for the characterization of the Li_2S/MC composite electrode, by the supporting of this technique displayed an open circuit potential at 3.0 V for pristine S/MC composite and the cathode electrode exhibited into two peaks at 2.4 and 1.1 V *vs* Li/Li^+ (Fig.8B). The electrode plays an important role for the manufacturing of low cost and commercially available in LIB. A systematic analysis of Na, Mg, Ca, Al and K storage on the nano sheetable MXene electrode, which can be fabricated by the first principles simulation method. MXene nanosheet was used as the anode for the electrochemical characterization of multilayer $Ti_3C_2T_x$ (T = O, F/OH), the CV curve showed their irrespective peaks of 1.2 V *vs* Na^+/Na and 1.5 V vs K^+/K observed during the electrolysis. This experiment was clearly explained the feasibility of Na^+ and K^+ interactions with MXene, O-terminated and unmodified MXene electrodes showed promising electro active materials for the study of high capacitive storage batteries [90].

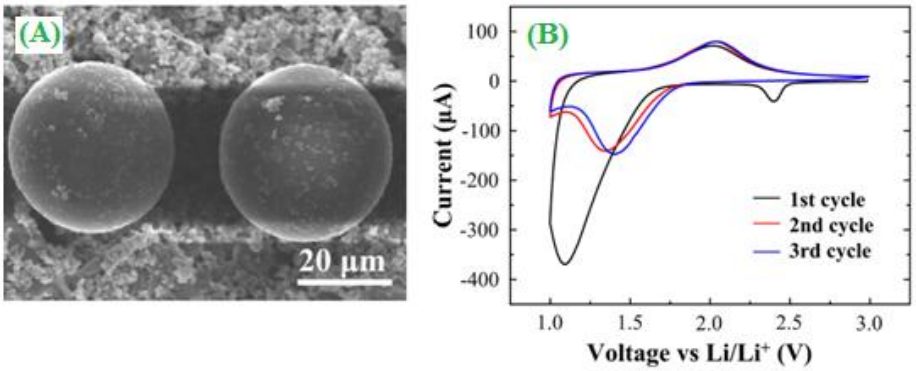

Figure 8. SEM image of the SLMP-sprinkled S/MC electrode film (B) Cyclic voltammograms and discharge/charge voltage profiles of the electrodes in the first three cycles at 0.1C for the pristine S/MC. ("Reprinted with permission from (*ACS Nano 7 (2013) 10995-11003*). Copyright (*2013*) American Chemical Society").

Self-assembled method was used as another viable approach in the preparation of three-dimensional mesoporous iron oxide nanoparticle clusters (MIONCs). The iron oxide particle size about 11-12 nm, the electrochemical analysis of mesoporous iron oxide anode electrode material, which was confirmed the oxidation species of Fe^0 to Fe^{2+} (1.66 V) and Fe^0 to Fe^{3+} (1.87 V). Although, the most important electrode catalyst of MIONCs, which was delivered an active electrode and excellent cyclic stability in LIB [91]. A simple chemical bath method has been employed for the synthesis of interconnected aligned nickel-cobalt oxide nanosheet array plays a significant role in electrochemical (LIB) applications. The nanosheet array electrode was characterized by charge/discharge and cyclic voltammetry analysis, the exhibited initial charge capacity value of 798 mAh g^{-1} at 0.1 A g^{-1} [92].

6.2. Electrochemical impedance spectroscopy

In order to the study of boron-based anion receptors [0.07M bis(1,1,1,3,3,3-hexafluoro isopropyl) pentafluorophenyl boronate have been evaluated from the electrolyte additive in LIB. By the addition of anion receptor, the capacity retention significantly increased the interfacial impedance and the promoted electrochemical decomposition of the electrolyte [93]. A L-cysteine-assisted layered based MoS_2/graphene composite has been prepared by solution-phase method.

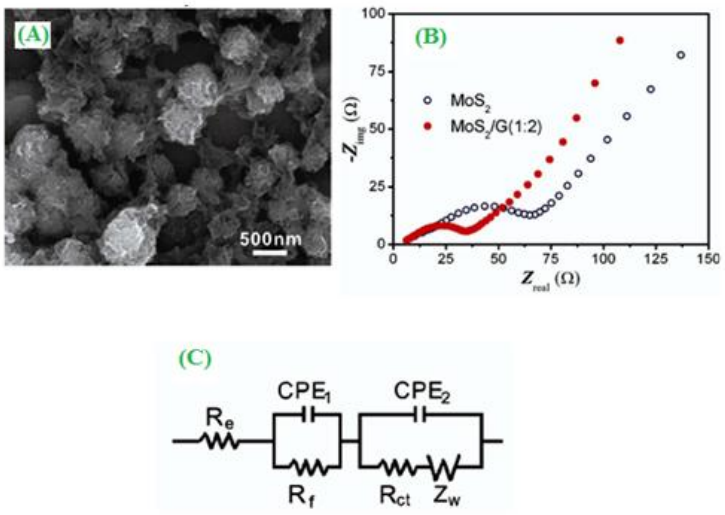

Figure 9. (A) SEM images of as-prepared MoS_2/G (1:2) (B) Nyquist plots of MoS_2 and MoS_2/G (1:2) electrodes obtained by applying a sine wave with amplitude of 5.0 mV over the frequency range from 100 kHz to 0.01 Hz (C) equivalent circuit model of the studied system. CPE represents the constant phase element, ZCPE = $\{Q(j\omega)n\}^{-1}$, $0 \leq 0 \leq 1$. ("Reprinted with permission from (*ACS Nano 5 (2011) 4720-4728*). Copyright (*2011*) American Chemical Society").

The as-prepared 3D sphere-like morphology of MoS_2/G (1:2 ratios) composite was annealed (800° C) under H_2/N_2 atmospheric condition for 2 h. The AC impedance equivalent circuit model of MoS_2/G, the internal resistance was associated with Warburg impedance. By this investigated modelling AC impedance spectroscopy, the charge-transfer resistance (R_{CT}) value of MoS_2/G (1:2)

electrode of 13.6 Ω, which was significantly reduced the unmodified MoS_2 (40.76 Ω) electrode (Fig.9) [94]. Similarly, Wu *et al* [95] developed a super high rate of nitrogen and boron doped graphene electrode were used as the promising anode catalyst for high performance studies in LIB. From the Nyquist plots were analyzed that the N_2 and B-doped graphene catalyst exhibited the charge-transfer resistance (R_{CT} = 63.99Ω and 59.88Ω) value, which was lower than that of the pristine graphene electrode (R_{CT} = 87.33Ω).

However, the application of silicon nanowire had attracted and considerable interest in the investigation of electrochemical performance by EIS, the estimated R_{np} magnitude displayed higher than that of R_{sur}/R_d [96]. Chen *et al* [97] have also demonstrated the role of a novel three-dimensional Tobacco mosaic virus fabricated with the silicone anode to achieve their specific capacity value (3300 mAh g^{-1}), which was 10-fold higher capacity value than the graphite anode. The Nyquist plot of biologically template nanocomposite, the impedance semi-circle region was greatly reduced. For the first time, nano homogeneous and multi-layered porous graphite composite electrode, which have applied at different electrode potential by electrochemical impedance spectroscopy (EIS) for LIB [98].

6.3. Ionic conductivity

Electro spinning polymerization has now become a popular method for the preparation of poly(ethylene oxide) and poly(vinylidinefluoride) based polymer gel electrolyte (PEG). The PEG has mainly focused for the measurement of ionic conductivity by using AC impedance technique. The observed ionic conductivity of PEG of 4.9 x 10^{-3} S cm^{-1} at lower temperature (25° C). This was clearly explained that, the incorporation of LiTFSI significantly reduced their electrolyte resistance and enhanced the ionic mobility of Li^+ ions [99]. The enhanced ionic conductivity of borate based film 4PAN-10EC/PC-4$LiBF_4$ (Polyacronitrile, ethylene carbonate and propylene carbonate) and 4PAN-10PEGB-4$LiCF_3SO_3$ (Polyethylene glycol borate ester) electrodes exhibits good conductivity and wide potential windows of electrochemical application. The lithium ion based borate film electrode mainly depends upon the frequency and various temperatures. These types of films were cut into disk like (Sandwich diameter 10 nm) platinum electrode. From the AC impedance analysis of 4PAN-10EC/PC-4$LiBF_4$ and 4PAN-10PEGB-4$LiCF_3SO_3$ polymer based electrodes, when increasing temperatures lead to faster moment of ion and higher ionic conductivity [100]. Poly(methylmethacrylate) (PMMA)-polyethylene oxide (PEO) hybrid polymer electrolyte have shown in interesting ionic conductivity and good mechanical stability in LIBs. By this type of ionic conducting membrane can be modified with PMMA, PEO and dimethyl phthalate (DMP) were optimized at room temperature (303 K) and the resulted dry plasticized film conductivity value of 6.4 x 10^{-5} S cm^{-1} [101]. The components of ternary polymer electrolyte (PEG, PEO, network cellulose (NC) and $LiClO_4$) PEG:PEO:NC (70:20:10 wt%) possess for the improvement of energy storage materials, the thermally optimized sample range of 60-120° C. The higher strength of ternary polymer electrolyte was exhibited thermal, mechanical stability and demonstrated the ionic conductivity of 10^{-4} S cm^{-1} [102]. However, the most lithium bis(oxalato)borate (LiBOB)-doped silyl solvent blend electrolyte has been used in LIB. The following parameters were induced the ionic conductivity of the polymer based electrolytes, such as salt

concentrations, solvent composition and temperatures, respectively. Vogel-Tammon-Flucher (VTF) equation have applied for the study of conductivity and viscosity, 0.8 M optimal salt-loading electrolyte yielded highest ionic conductivity σ_{25} of 1.99 ± 0.02 mS cm^{-1} [103]. Feng *et al* [104] have used a freestanding, self-assembled ternary membrane encompasses with hyper branched polyether, PVDF-HFP and ionic liquid. The thermally stable (320° C) polymer electrolyte membrane were exhibited the ionic conductivity can reach around 1.37 x 10^{-3} S cm^{-1}.

6.4. Cationic-charge transfer

Shinova *et al* [105] employed the lithium cobalt-nickel-manganese ($LiCo_{1/3}Ni_{1/3}Mn_{1/3}O_2$) oxide was optimized the prepared temperature between 850 to 900° C. The cationic (Li^{2+} and Ni^{2+}) distorter has been determined by Rietveld structural model and the cationic distribution layer was measured by both conventional and high-frequency electron paramagnetic resonance spectroscopy (EPR). The prepared increasing temperatures (850 to 900° C) could possess a non-homogeneous cationic distribution and the significant electrochemical performance in LIB. Lithium cobaltate ($LiCo_{1-y}B_yO_2$) as a cathode positive (B^{3+} and Co^{3+}) electrode materials, which can be applied in rechargeable LIB. The solid states of electrode's structural properties have also been optimized by XRD technique. The cyclic discharged capacity of Li/$LiCo_{1-y}B_yO_2$ catalyst almost independent, but in the case of boron-doped electrode catalyst for the improvement of cyclic performance and favour the lattice adsorption of lithium and the ionic transfer of $Li_{0.5}CoO_2$ [106]. The enhanced discharging capacity of $LiFePO_4$ cathode, which was modified with a small amount of V_2O_5. The resulted pristine $Li_{1-x-v}V_xFePO_4$ cathode, cation (Li^+ ion) can move faster between anode and cathode electrodes. This was clearly explained that, the decreasing of polarization effect and the enhancement of both conductivity and electrochemical properties [107]. Nevertheless, recent studies have used Prussian blue nanomaterials and nickel hexacyanoferrate allowed for the reversible insertion of divalent ions like Mg^{2+}, Ca^{2+}, Sr^{2+} and Ba^{2+}, the creation of a new type of battery, potentially safer and cheaper than LIB. The cationic ions (Mg^{2+}, Ca^{2+}, Sr^{2+} and Ba^{2+}) have been characterized by the cyclic voltammetry method, the reversible insertion of ion concentration electrolytes after the discharged capacity reached around 11, 41, 64 and 73% for Mg^{2+}, Ca^{2+}, Sr^{2+} and Ba^{2+} respectively [108]. In particulate, a new cross-linked polyurethane acrylate (PUA) has been synthesized by using hexamethylene diisocyanate, hexamethylene diisocyanate/poly(ethylene glycol)-based polymers can be modified with hydroxyl butyl methacrylate (HBM). Whereas, lithium ion can be interacted with soft and hard segments of the host polymer with lithium perchlorate ($LiClO_4$). The predominant electrochemical ion-pairs of $LiClO_4$ contact, which were analyzed by A.C. conductivity and different scanning calorimetric (DSC) methods [109]. The development of low cost, newly formed lithium based $Li(Ni_{1/3}Mn_{1/3}Co_{1/3-x}M_x)O_2$, (M = Mg, Fe, Al and x = 0 to 0.33) cathode material for the use of rechargeable LIB by Pechini method. The substituted metal based (Fe and Mg) composition exhibited higher electrical conductivity than the $Li(Ni_{1/3}Co_{1/3}Mn_{1/3})O_2$ and the discharged capacity of Fe for 122 and Mg for 125 mAh g^{-1} respectively [110].

6.5. Charge-discharge

A single crystalline hematite (α-Fe_2O_3) nano rod is an attractive anode electrode material offers superior safety and excellent reversibility in LIB. The hydrothermally synthesized particles (nano rod) diameters ~40 nm and its average length ~400 nm (Fig.10B).

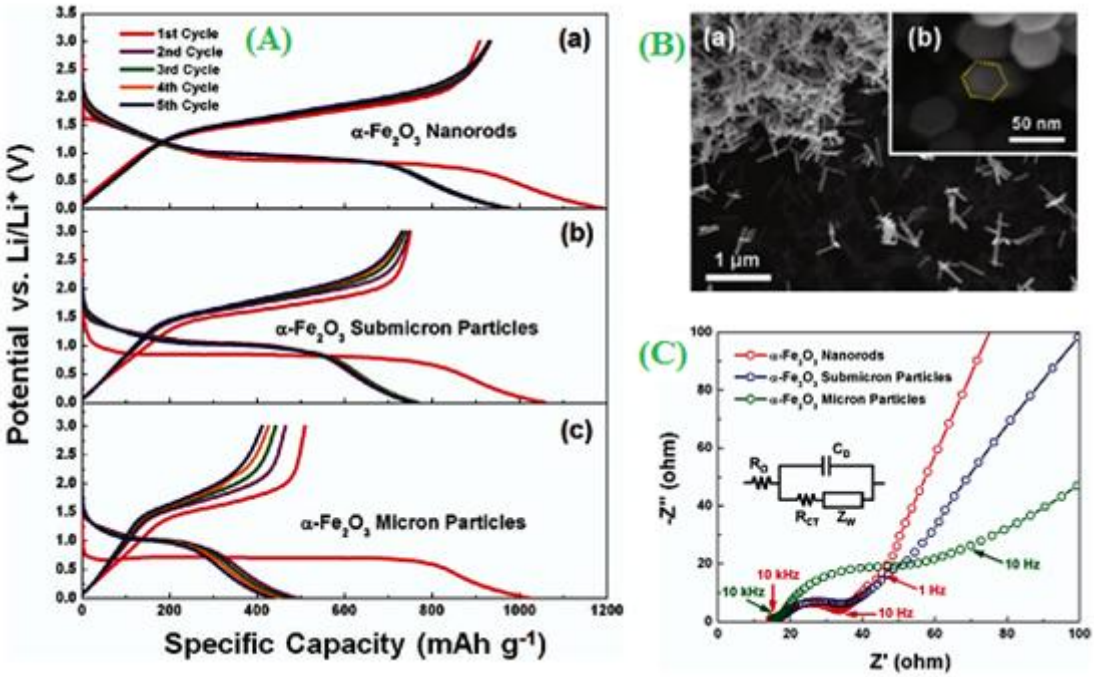

Figure 10. (A) Voltage profiles of electrodes made with (a) α-Fe_2O_3 nanorods, (b) α-Fe_2O_3 sub-micrometer particles, and (c) α-Fe_2O_3 micrometer-sized particles. All electrodes cycled at 0.2 C rate (201 mA g^{-1}). (B) SEM images of α-Fe_2O_3 nano rods (a) at a low magnification and (b) end-view at a high magnification. (C) Electrochemical impedance spectroscopy of electrodes with α-Fe_2O_3 nanorods, sub-micrometer particles α-Fe_2O_3, and micro-meter sized particles α-Fe_2O_3. ("Reprinted with permission from (*J. Phys. Chem. C 2 (2011) 2885-2891*). Copyright (*2011*) American Chemical Society").

The initial voltage discharge-charge curves of α-Fe_2O_3 nano rod anode; the first cycle plateau occurs at 1.6 V *vs* Li/Li^+, the stabilized anode materials, initial reversible specific capacity value of 908 mAh g^{-1} (Fig.10A). In Fig.10C, the other type of electrochemical analysis (EIS) could be attributed to the smaller semi-circle diameter region of hematite nano rod electrode exhibits higher electrochemical performance in LIB [111]. The as-synthesized (Ball milling) method of organic tetra lithium salts of 2,5-dihydroxy terephthalic acid ($Li_4C_8H_2O_6$) is a promising active positive or negative electrode material for use in rechargeable LIB. The remarkable being an inexpensive lamellar morphology of nano sheets reported the higher batteries capacity value of 223 mAh g^{-1} [112]. Furthermore, considerable effort has been made to develop a layered structure of molybdenum (Oxy)-pyrophosphate (δ-$(MoO_2)_2)P_2O_7$ electrode was synthesized by heating method. Notably, molybdenum based phosphate electrode exhibit multi-electron redox center, the resulted reversible intercalated 1.9 lithium displayed 110 mAh g^{-1} at 2.3 and 4.0 V [113].Besides, the solid state of lithium-ion thin film

can be modified with Nb_2O_5 negative electrode by sputter-coating method. The electrochemical characterization study of Nb_2O_5 electrode was investigated by charge-discharge method, the thinnest (100 nm) coated negative electrode displayed their capacity properties value in the range of 310-380 mAh cm^{-3} [114]. However, a uniform and narrow size distributed $LiNi_{0.5}Mn_{1.5}O_4$ cathode electrode material has been widely used in LIB. The ethylene glycol (EG)-assisted co-precipitation method prepared lithium based electrode showed the smaller semi-circle region, lower polarization potential and higher reversibility [115]. Recently, Kweon *et al* [116] reported that, polycrystalline powder of $Li_xNi_{0.85}Co_{0.15}O_2$ has a high discharged capacity value around 170 mAh g^{-1} by using *I-V* characteristic charge-discharge method. While, the anode crystalline catalyst had large surface area, smaller particle size and higher carbon content for LIB.

6.7. Cyclic performance

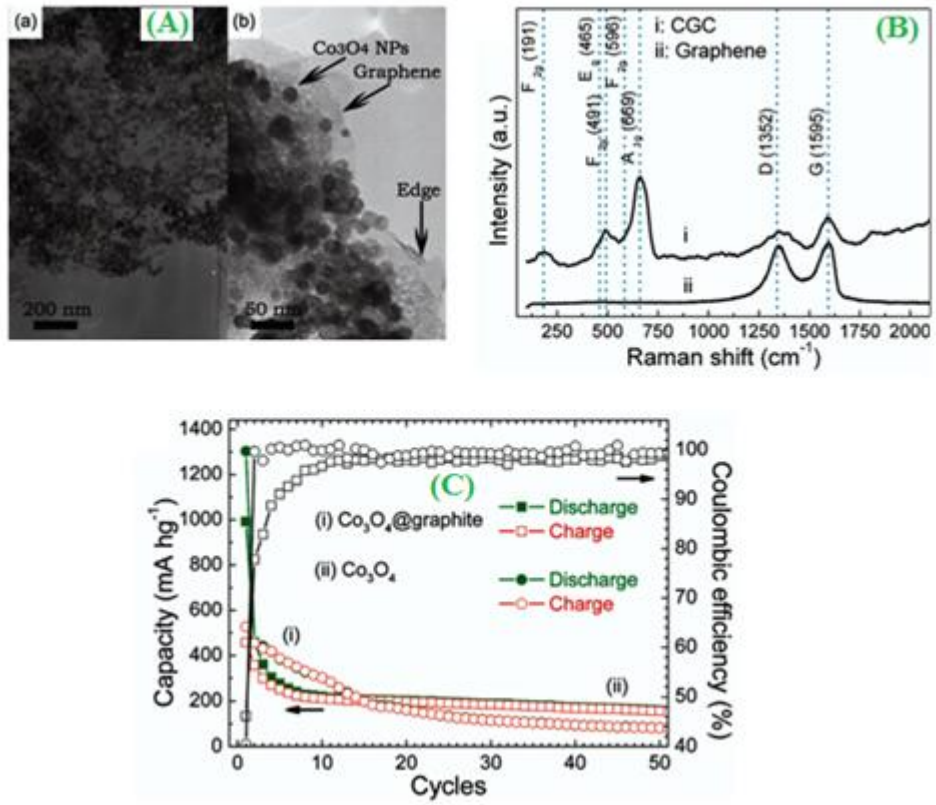

Figure 11. (A) Typical TEM (a, b) images of CGC (B) Raman spectra of the CGC and graphene (C) cyclic performances of electrodes fabricated byCo_3O_4@graphite andCo_3O_4 at a current rate of 0.2C. ("Reprinted with permission from (*Inorg. Chem. 50 (2011) 1628-1632*). Copyright (*2011*) American Chemical Society").

Figure.11 shows, cobalt oxide (Co_3O_4) nano particles (NPs) has been used as the chemical deposition method for the homogeneous dispersion onto the graphene sheets (Co_3O_4@graphene) (CGC) composite. From the analytical characterization (Raman spectra) of CGC and graphene electrodes were observed Raman shift in 191, 491 and 596 cm^{-1} (F_2g vibration mode of Co_3O_4) and the

shift at 465 & 669 cm^{-1} (E_g & A_{1g} mode). The performance studies of CGC anode electrode materials have been carried out by using charge-discharge method at high current density. This can be attributed to an extraordinary electronic transition property, high surface area and highly conductive matrix in LIB [117]. Qiu and co-workers reported a hydrogenated blue rutile TiO_2 nanoparticle (Blue TiO_2) provided the significant energy capacity and better LIB performance than white TiO_2 electrode i.e. The blue TiO_2 discharged capacity of 179.8 & 129.2 mAh g^{-1}, which was higher value than that of white TiO_2 (119.6 & 55 mAh g^{-1}) electrode [118]. More recently, organic monolayer coated germanium (Ge-C) nanowire anode have been considerably as a good electrode catalyst in high performance thermal stable (55° C), high rate and good reversibility of LIB. Substantially, the important application of the structure associated with functionalized Ge nanowire and Li ion reaction [119]. Among various methods, one of the effective hydrothermal methods for the synthesis of nano plate MnO_2/reduced graphite oxide (MnO/RGO) composite powder for the estimation of the structural and electrochemical properties. A high specific surface area (42.4 m^2 g^{-1}) of MnO/RGO composite can be modified with 13.19 wt % ratio of RGO delivered the reasonable different capacity values of 855, 842, 821, 737 and 600 mAh g^{-1} at different applied current densities (0.16, 0.41, 0.8, 1.6 and 3.2 A g^{-1}) [120]. In general, the most commonly used lithium ion phosphate ($LiFePO_4$), which was interconnected with mesoporous carbon nano sheets ($LiFePO_4$@CNTs/CNSs) composite by in situ soft-template method. Rapidly, $LiFePO_4$@CNTs/CNSs composite reported the greater rate capacity and admirable cyclic stability than the LFP/CNSs electrode [121]. Liu *et al* [122] investigated the LIB studies using porous tremella-like molebdenum disulfide based polyaniline (MoS_2/PANI) composite as the electrode catalyst in acidic solution. The LIB has been reported on a polyaniline modified highly porous MoS_2 electrode in 1M HCl. The significant of electrode sites for LIB delivered the highest capacity value of 915 mAh g^{-1}.

6.8. Cyclic stability

The scalable preparation of size-tunable and defect-free graphene (+ve) (df-G) electrode, which can be wrapped with a positively charged Co_3O_4; pyridine was used as the most effective solvent for the preparation method. The morphological study was evaluated by the tight wrapped df-G/Co_3O_4 composite showed bundle-like shape and the agglomerated particle size around 200-400 nm. The electrode stability has been optimized by cyclic voltammetry and charge-discharge methods, the obtained cyclic stability of df-G/Co_3O_4 composite highest reversible capacity value of 1050 mAh g^{-1} at 500 mA g^{-1} for 200 cycles as shown in Fig.12 [123]. The arc-discharged method has been used for the fabrication of tin based multi-walled carbon nanotube nano capsules (Sn-CNTs NCs). The large storage capacity of Sn-CNTs NCs was investigated by cyclic performance studies, the main observed initial cycle of Sn NPs anode exhibit higher reversible capacity values (935 mAh g^{-1}), whereas in the cause of 10^{th} cycles, Sn-CNTs NCs electrode calculated the capacity value of 612 mAh g^{-1} [124]. The high performance of carbon-TiO_2 (C-TiO_2) nanocomposite anode was fabricated by a simple and cheap carbonization method.

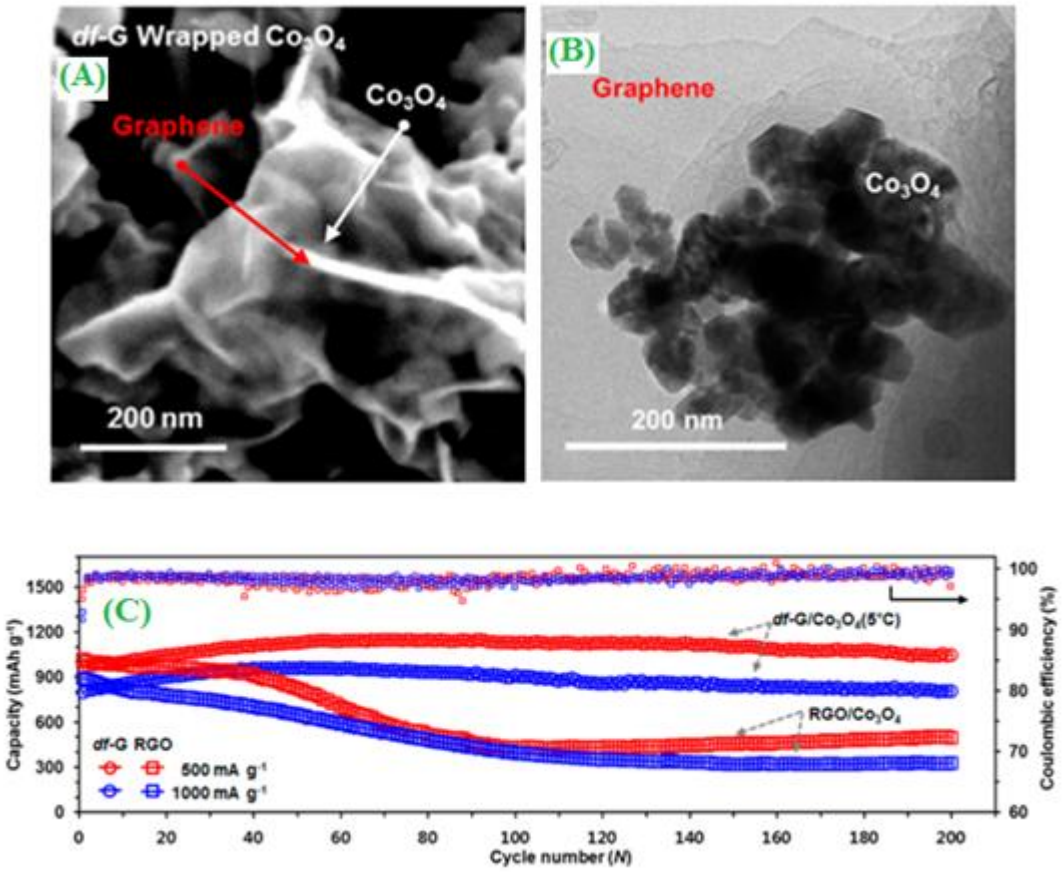

Figure 12. (A&B) SEM and TEM images of df-G/Co_3O_4 composite (C) Comparison of cycling performance of df-G/Co_3O_4 and RGO/Co_3O_4 at current densities of 500 and 1000 mA g^{-1}. ("Reprinted with permission from (*Nano Lett., 14 (2014) 4306-4313*). Copyright (*2014*) American Chemical Society").

The anode electrode material's maximum observed initial discharged capacity value around 231 mAh g^{-1} and the retained capacity value of 173 mAh g^{-1} after the 100^{th} cycles, because of its significant cyclic stability and excellent electrochemical performance in LIB [125]. A new type of amorphous Si@SiO_x/Cr/Carbon (a-Si@SiO_x/Cr/C) composite served as a host anode electrode material for an electrochemical device application. The optimized chromium content composite made high performance capacity (810 mAh g^{-1}) and excellent cyclic stability (200 cycles, 100 % retention) [126]. Specifically, hydrothermal method has been used for the fabrication of grass-like Co_3O_4 nanowire arrays (Co_3O_4 NWAs) on titanium foil electrode. The synthesized Co_3O_4 NWAs diameter ranges around 70-100 nm, the marvelous specific capacity (1031) and long durability (100 cycles) of electrochemical reaction in LIB [127]. A co-crystallization reverse micellar microemulsion is a viable method to form lithium-rich oxide ($Li[Li_{0.9}Mn_{0.32}Co_{0.42}]O_2$) nano rod and the obtained electrode morphological length about 1 μm and their diameter around 200 nm. The hierarchical porous structure of the electrode substrate resulted larger discharged capacity and better cyclic stability in LIB applications [128].

7. CONCLUSIONS

As can be the discussed review article, the recent progress in the fabrication of novel electrode materials via simple methods for LIB applications. The following types of electrode materials (Carbon fiber, MWCNT, metal oxides, conducting polymers and nano composites) can offer larger electrode surface area, different size and shape of the morphological structure. These kinds of electrode materials were highly electro active, larger discharged specific capacities and longer durability in LIB. The number of reported literature for the high potential energy storage devices can achieve more power generation in the field of electrochemistry. In the general strategy of LIB undoubtedly will contribute to the future energy technology such as excellent compatibility and safety usage in the portable electronic devices.

ACKNOWLEDGEMENT
We gratefully acknowledged, The Management and Chemistry Department Staff members, The Madura College, Madurai, Tamil Nadu, India. And also we thankful to Mr.Abhijit Manna, JRF, SBS, DAB & P, MKU, for his valuable discussion in this article.

References

1. C. Zhang, Y. Liang, L. Yao, Y. Qiu, *J. Alloys Compd., 627(2015) 91-100.*
2. H. Huang, W.K. Zhang, X.P. Gan, *Mater. Chem. Phys., 104* (*2007) 271-275.*
3. L. Kavan, R. Bacsa, M. Tunckol, P. Serp, S.M. Zakeeruddin, F.L. Formal, M. Zukalova, M. Graetzel, *J. Power Sources, 195 (2010) 5360-5369.*
4. M. Lübke, I. Johnson, N.M. Makwana, D. Brett, P. Shearing, Z. Liu, J.A. Darr, *J. Power Sources, 294 (2015) 94-102.*
5. C. Chen, S.H. Lee, M. Cho, Y. Lee, *Mater. Lett., 140 (2015) 111-114.*
6. H. Guo, L. Liu, Q. Wei, H. Shu, X. Yang, Z. Yang, M. Zhou, J. Tan, Z. Yan, X. Wang, *Electrochim. Acta, 94(2013)113-123.*
7. Q.G. Shao, W.M. Chen, Z.H. Wang, L. Qie, L.X. Yuan, W.X. Zhang, X.L. Hu, Y.H. Huang, *Electrochem. Commun., 13 (2011) 1431-1434.*
8. H. Xia, D. Zhu, Y. Fu, X. Wang, *Electrochim. Acta, 83(2012)166-174.*
9. B. Das, A. Pohl, V.S.K. Chakravadhanula, C. Kübel, M. Fichtner, *J. Power Sources, 267(2014)203-211.*
10. F. Wu, G. Tan, J. Lu, R. Chen, L. Li, K. Amine, *Nano Lett., 14 (2014) 1281-1287.*
11. J.H. Kim, J.H. Kim, E.S. Coi, H.K. Yu, J.H. Kim, Q. Wu, S.J. Chun, S.Y. Lee, S.Y. Lee, *J. Power Sources 242 (2013) 533-540.*
12. Y. Jiang, Z.J. Jiang, S. Cheng, M. Liu, *Electrochim. Acta 146 (2014) 437-446.*
13. S. Ni, T. Li, X. Lv, X. Yang, L. Zhang, *Electrochim. Acta 91 (2013) 267-274.*
14. Z. Zheng, Y. Fu, X. Yang, Y. Qu, Q. Li, *Electrochim. Acta 168 (2015) 285-291.*
15. Z. Edfouf, C.F. Georges, F. Cuevas, M. Latroche, T. Hezeque, G. Caillon, C. Jordy, M.T. Sougrati, J.C. Jumas, *Electrochim. Acta 89 (2013) 365-371.*
16. R. Rohan, Y. Sun, W. Cai, Y. Zhang, K. Pareek, G. Xu, H. Cheng, *Solid State Ionics, 268 (2014) 294-299.*
17. I. Camean, P. Lavela, J.L. Tirado, A.B. Garcia, *Fuel, 89 (2010) 986-991.*
18. G. Wang, X. Shen, J. Yao, *J. Power Sources 189 (2009) 543-546.*

19. L. Wang, L.C. Zhang, J.X. Cheng, C.X. Ding, C.H. Chen, *Electrochim. Acta 102 (2013) 306-311.*
20. K.J. Babu, A. Zahoor, K.S. Nahm, R. Ramachandran, M.A.J. Rajan, G. Gnana kumar, *J. Nanopart. Res. 16 (2014) 2250.*
21. R. Ramachandran, V. Mani, S.M. Chen, R. Saraswathi, B.S. Lou, *Int. J Electrochem. Sci. 8 (2014) 11680.*
22. R. Ramachandran, V. Mani, S.M. Chen, G. Gnana kumar, M. Govindasamy *Int. J. Electrochem. Sci. 10 (2015) 859-869.*
23. R. Ramachandran, V. Mani, S.M. Chen, G. Gnana kumar, P. Gajendran, N.B. Devi, R. Devasenathipathy *Int. J Electrochem. Sci.10 (2015) 3301-3318.*
24. S.M. Chen, R. Ramachandran, V. Mani, R. Saraswathi *Int. J Electrochem. Sci. 9 (2014) 4072.*
25. J. Liu, K. Song, C. Zhu, C.C. Chen, P.A.V. Aken, J. Maier, Y. Yu, *ACS Nano 8 (2014) 7051-7059.*
26. S. Wang, X. Zhao, T. Cochell, A. Manthiram, *J. Phys. Chem. Lett., 3 (2012) 2164-2167.*
27. A. Vu, A. Stein, *Chem. Mater., 23 (2011) 3237-3245.*
28. K. Evanoff, J. Benson, M. Schauer, J. Benson, M. Schauer, I. Kovalenko, D. Lashmore, W.J. Ready, G. Yushin, *ACS Nano 6 (2012) 9837-9845.*
29. Z. Jiang, Z.J. Jiang, X. Tian, L. Luo, *Electrochim. Acta 146 (2014) 455-463.*
30. C. Wang, G. Shao, Z. Ma, S. Liu, W. Song, J. Song, *Electrochim. Acta 130 (2014) 679-688.*
31. Y. Wang, L. Tian, Z. Yao, F. Li, S. Li, S. Ye, *Electrochim. Acta 163 (2015) 71-76.*
32. P. Zhang, J. Qiu, Z. Zheng, G. Liu, M. Ling, W. Martens, H. Wang, H. Zhao, S. Zhang, *Electrochim. Acta 104 (2013) 41-47.*
33. J. Jin, Z.Q. Shi, C.Y. Wang, *Electrochim. Acta 141 (2014) 302-310.*
34. S.M. Abbas, S.T. Hussain, S. Ali, N. Ahmad, N. Ali, K.S. Munawar, *Electrochim. Acta 105 (2013) 481-488.*
35. J. Ye, A.C. Baumgartel, Y.M. Wang, J. Biener, M.M. Biener, *ACS Nano 9 (2015) 2194-2202.*
36. Z. Zheng, J. Liu, D. Lv, Q. Kuang, Z. Jiang, Z. Xie, R. Huang, L. Zheng, *J. Solid State Chem. 183 (2010) 600-605.*
37. C.M. Doherty, R.A. Caruso, B.M. Smarsly, P. Adelhelm, C.J. Drummond, *Chem. Mater., 21 (2009) 5300-5306.*
38. S.R. Gowda, V. Pushparaj, S. Herle, G. Girishkumar, J.K. Gordon, H. Gullapalli, X. Zhan, P.M. Ajayan, A.L.M. Reddy, *Nano Lett., 12 (2012) 6060-6065.*
39. Z. Jiang, C. Li, S. Hao, K. Zhu, P. Zhang, *Electrochim. Acta 115 (2014) 393-398.*
40. G. Qiu, Q. Ma, C. Wang, *Electrochim. Acta 115 (2014) 407-415.*
41. Y. Xia, Z. Xiao, X. Dou, H. Huang, X. Liu, R. Yan, Y. Gan, W. Zhu, J. Tu, W. Zhang, X. Tao, *ACS Nano 7 (2013) 7083-7092.*
42. L. Shen, H. Li, E. Uchaker, X. Zhang, G. Cao, *Nano Lett., 12 (2012) 5673-5678.*
43. J. Hwang, S.H. Woo, J. Shim, C. Jo, K.T. Lee, J. Lee, *ACS Nano 7 (2013) 1036-1044.*
44. J. Lin, Z. Peng, C. Xiang, G. Ruan, Z. Yan, D. Natelson, J.M. Tour, *ACS Nano 7 (2013) 6001-6006.*
45. Y. Zhang, Y. Liu, M. Liu, *Chem. Mater., 18 (2006) 4643-4646.*
46. P.R. Abel, Y.M. Lin, H. Celio, A. Heller, C.B. Mullin, *ACS Nano 6 (2012) 2506-2516.*
47. H. Lv, S. Qiu, G. Lu, Y. Fu, X. Li, C. Hu, J. Liu, *Electrochim. Acta 151 (2015) 214-221.*
48. M.H. Alfaruqi, A.K. Rai, V. Mathew, J. Jo, J. Kim, *Electrochim. Acta 151 (2015) 558-564.*
49. C. Arbizzani, A. Balducci, M. Mastragostino, M. Rossi, F. Soavi, *J. Electroanal. Chem.,* 553 (2003) 125-133.
50. P. Sharma, D. Damien, K. Nagarajan, M.M. Shaijumon, M. Hariharan, *J. Phys. Chem. Lett., 4 (2013) 3192-3197.*
51. M. Wilamoska, M.G. Zajac, R. Riedel, *J. Power Sources 244 (2013) 80-86.*
52. G. Liu, J. Kaspar, L.M. Reinold, R.G. Zajac, R. Riedel, *Electrochim. Acta 106 (2013) 101-108.*

53. Y.S. Zhu, X.J. Wang, Y.Y. Hou, X.W. Gao, L.L. Liu, Y.P. Wu, M. Shimizu, *Electrochim. Acta 87 (2013) 113-118.*
54. X. Wang, Z. Liu, C. Zhang, Q. Kong, J. Yao, P. Han, W. Jiang, H. Xu, G. Cui, *Electrochim. Acta 92 (2013) 132-138.*
55. Y. Wang, F. Su, C.D. Wood, X.S. Zhao, *Ind. Eng. Chem. Res., 47 (2008) 2294-2300.*
56. P. Carol, P. Ramakrishnan, B. Jhon, G. Cheruvally, *J. Power Sources 196 (2011) 10156-10162.*
57. L. Zhao, H. Chen, Y. Wang, H. Che, P. Gunawar, Z. Zhang, H. Li, F. Su, *Chem. Mater., 24 (2012) 1136-1142.*
58. W. Lu, K. Xie, Z.X. Chen, Y. Pan, C.M. Zheng, *J. Fluorine Chem., 161 (2014) 110-119.*
59. H.G. Zahmatkesh, M. Javanbakht, M. Ghaemi, *J. Power Sources 284 (2015) 339-348*
60. J. Guo, F. Li, Y. Sun, X. Zhang, L. Tang, *Electrochim. Acta 167 (2015) 32-38.*
61. M. Gu, I. Belharouak, A. Genc, Z. Wang, D. Wang, K. Amine, F. Gao, G. Zhou, S. Thevuthasan, D.R. Baer, J.G. Zhang, N.D. Browning, J. Liu, C. Wang, *Nano Lett., 12 (2012) 5186-5191.*
62. H. Yang, T. Song, L. Liu, A. Devados, F. Xia, H. Han, H. Park, W. Sigmund, K. Kwon, U. Paik, *J. Phys. Chem. C 117 (2013) 17376-17381.*
63. D.T. Welna, D.A. Stone, H.R. Allcock, *Chem. Mater., 18 (2006) 4486-4492.*
64. T. Song, J. Xia, J.H. Lee, D.H. Lee, M.S. Kwon, J.M. Choi, J. Wu, S.K. Doo, H. Chang, W.I. Park, D.S. Zhang, H. Kim, Y. Huang, K.C. Hwang, J.A. Roger, U. Paik, *Nano Lett., 10 (2010) 1710-1716.*
65. M. Xie, R. Luo, R. Chen, F. Wu, T. Zhao, Q. Wang, L. Li, *ACS Appl. Mater. Interfaces 7 (2015) 10779-10784.*
66. F. Wu, N. Li, Y. Su, L. Zhang, L. Bao, J. Wang, L. Chen, Y. Zheng, L. Dai, J. Peng, S. Chen, *Nano Lett., 14 (2014) 3550-3555.*
67. C.S. Cheng, W.R. Liu, F.M. Wang, *Electrochim. Acta 106 (2013) 425-431.*
68. Y.J. Nam, S.J. Cho, D.Y. Oh, J.M. Lim, S.Y. Kim, J.H. Song, Y.G. Lee, S.Y. Lee, Y.S. Jung, *Nano Lett., 15 (2015) 3317-3323.*
69. P. Abellan, B.L. Mehdi, L.R. Parent, M. Gu, C. Park, W. Xu, Y. Zhang, I. Arslan, J.G. Zhang, C.M. Wang, J.E. Evans, N.D. Browning, *Nano Lett., 14 (2014) 1293-1299.*
70. P.X. Yang, L. Liu, L. Li, J. Hou, X. Ren, M. An, N. Li, *Electrochim. Acta 115 (2014) 454-460.*
71. Z. Zeng, B. Wu, L. Xiao, X. Jiang, Y. Chen, X. Ai, H. Yang, *J. Power Sources 279 (2015) 6-12.*
72. Q. Wang, B. Zhang, J. Zhang, Y. Yu, P. Hu, C. Zhang, G. Ding, Z. Liu, C. Zong, G. Cui, *Electrochim. Acta 157 (2015) 191-198.*
73. W. Lu, K. Xie, Z. Chen, S. Xiong, Y. Pan, C. Zheng, *J. Power Sources 274 (2015) 676-684.*
74. J.G. Zhu, Z.C. Sun, X.Z. Wei, H.F. Dai, *J. Power Sources 274 (2015) 990-1004.*
75. K.M. Kim, N.V. Ly. J.H. Won, Y.G. Lee, W.I. Cho, J.M. Ko, R.B. Kaner, *Electrochim. Acta 136 (2014) 182-188.*
76. W. Lu, K. Xie, Y. Pan, Z.X. Chen, C.M. Zheng, *J. Fluorine Chem., 156 (2013) 136-143.*
77. W. Zhang, D. Liu, *Electrochim. Acta 156 (2015) 53-59.*
78. M.S.K. Mutyala, J. Zhao, J. Li, H. Pan, C. Yuan, X. Li, *J. Power Sources 260 (2014) 43-49.*
79. S.J. Lee, J.G. Han, Y. Lee, M.H. Jeong, W.C. Shin, M. Ue, N.S. Choi, *Electrochim. Acta 137 (2014) 1-8.*
80. X. Ma, G. Ning, C. Qi, C. Xu, J. Gao, *ACS Appl. Mater. Interfaces 6 (2014) 14415-14422.*
81. L. Lang, Z. Xu, *ACS Appl. Mater. Interfaces 5 (2013) 1698-1703.*
82. W. Zhang, W. Zhou, J.H. Wright, Y.N. Kim, D. Liu, X. Xiao, *ACS Appl. Mater. Interfaces 6 (2014) 7292-7300.*
83. W.A. Ang, N. Gupta, R. Prasanth, S. Madhavi, *ACS Appl. Mater. Interfaces 4 (2014) 7011-7019.*
84. C.C. Li, Q.H. Li, L.B. Chen, T.H. Wang, *ACS Appl. Mater. Interfaces 4 (2012) 1233-1238.*
85. X. Shen, D. Mu, S. Chen, B. Wu, F. Wu, *ACS Appl. Mater. Interfaces 5 (2013) 3118-3125.*
86. D. Chen, G. Ji, Y. Ma, J.Y. Lee, J. Lu, *ACS Appl. Mater. Interfaces 3 (2011) 3078-3083.*

87. H. Zhou, S. Upreti, N.A. Chernova, G. Hautier, G. Ceder, M.S. Whittingham, *Chem. Mater., 23 (2011) 293-300.*
88. J. Liu, X. Yu, E. Hu, K.W. Nam, X.Q. Yang, P.G. Khalifah, *Chem. Mater., 25 (2013) 3929-3931.*
89. S. Zhang, Y. Chen, Y. Xu, F. Yi, Y. Zhu, Y. Liu, J. Yang, C. Wang, *ACS Nano 7 (2013) 10995-11003.*
90. Y. Xie, Y.D. Agnese, M. Naguib, Y. Gogotsi, M.W. Barsoum, H.L. Zhuang, P.R.C Kent, *ACS Nano 8 (2014) 9606-9615.*
91. S.H. Lee, S.H Yu, J.E. Lee, A. Jin, D.J. Lee, N. Lee, H. Jo, S. Shin, T.Y. Ahn, Y.W. Kim, H. Choe, Y.E. Sung, T. Hyeon, *Nano Lett., 13 (2013) 4249-4256.*
92. X. Huang, J. Wu, R. Guo, Y. Lin, P. Zhang, *Int. J. Hydrogen Energy 39 (2014) 21399-21404.*
93. Y. Qin, Z. Chen, H.S. Lee, X.Q. Yang, K. Amine, *J. Phys. Chem. C 114 (2010) 15202-15206.*
94. K. Chang, W. Chen, *ACS Nano 5 (2011) 4720-4728.*
95. Z.S. Wu, W. Ren, L. Xu, F. Li, H.M. Cheng, *ACS Nano 5 (2011) 5463-5471.*
96. R. Ruffo, S.S. Hong, C.K. Chan, R.A. Huggins, Y. Cui, *J. Phys. Chem. C 113 (2009) 11390-11398.*
97. X. Chen, K. Gerasopoulos, J. Guo, A. Brown, C. Wang, R. Ghodssi, J.N. Culver, *ACS Nano 4 (2010) 5366-5372.*
98. S.D. Xu, Q.C. Zhuang, L.L. Tian, Y.P. Qin, L. Fang, S.G. Sun, *J. Phys. Chem. C 115 (2011) 9210-9219.*
99. R. Prasanth, N. Shubha, H.H. Hng, M. Srinivasan, *J. Power Sources 245 (2014) 283-291.*
100. M. Kaynak, A. Yusuf, A. Aydin, M.U. Taskiran, *Electrochim. Acta 164 (2015) 108-113.*
101. S. Rajendran, R. Kannan, O. Mahendran, *J. Power Sources 96 (2001) 406-410.*
102. B.S. Lalia, Y.B. Samad, R. Hashaikeh, *Int. J. Hydrogen Energy 39 (2014) 2964-2970.*
103. W.V. Barth, A.P. Hueso, L. Zhou, L. Lyons, R. West, *J. Power Sources* 272 (2014) 190-195.
104. T. Feng, F. Wu, C. Wu, X. Wang, G. Feng, H. Yang, *Solid State Ionics 221 (2012) 28-34.*
105. E. Shinova, R. Stoyanova, E. Zhecheva, G.F. Ortiz, P. Lavela, J.L Tirado, *Solid State Ionics 179 (2008) 2198-2208.*
106. C.M. Julien, A. Mauger, H. Groult, X. Zhang, F. Gendren, *Chem. Mater., 23 (2011) 208-218.*
107. C.Y. Chang, H.C. Su, P.J. Wu, H.J. Liu, C.W. Hu, N. Sharma, V.K. Peterson, H.W. Hsieh, Y.F. Lin, W.C. Chou, C.H. Lee, J.F. Lee, B.Y. Shew, *J. Phys. Chem. C 116 (2012) 24424-24429.*
108. R.Y. Wang, C.D. Wesseles, R.A. Huggins, Y. Cui, *Nano Lett., 13 (2013) 5748-5752.*
109. P. Santhosh, T. Vasudevan, A. Gopalan, K.P. Lee, *J. Power Sources 160 (2006) 609-620.*
110. P.B. Samarasingha, A. Wijayasinghe, M. Behm, L. Dissanayake, G. Lindebergh, *Solid State Ionics 268 (2014) 226-230.*
111. Y.M. Lin, P.R. Abel, A. Heller, C.B. Mullins, *J. Phys. Chem. C 2 (2011) 2885-2891.*
112. S. Wang, L. Wang, K. Zhang, Z. Zhu, Z. Tao, J. Chen, *Nano Lett., 13 (2013) 4404-4409.*
113. B. Wen, N.A. Chernova, R. Zhang, Q. Wang, F. Omenya, J. Feng, M.S. Whittingham, *Chem. Mater., 25 (2013) 3513-3521.*
114. H. Nakazawa, K. Sano, T. Abe, M. Baba, N. Kumagi, *J. Power Sources 174 (2007) 838-842.*
115. T.F. Yi, Z.K. Fang, Y. Xie, Y.R. Zhu, L.Y. Zang, *Electrochim. Acta 147 (2014) 250-256.*
116. H.J. Kweon, G.B. Kim, H.B. Lim, S.S. Nam, D.G. Park, *J. Power Sources 83 (1999) 84-92.*
117. B. Li, H. Cao, J. Shao, G. Li, M. Qu, G. Yin, *Inorg. Chem., 50 (2011) 1628-1632.*
118. J. Qiu, S. Li, E. Gray,H. Liu, Q.F. Gu, C. Sun, C. Lai, H. Zhao, S. Zhan, *J. Phys. Chem. C 118 (2014) 8824-8830.*
119. F.W. Yuan, H.J. Yang, H.Y. Juan, *ACS Nano 6 (2012) 9932-9942.*
120. B.K. Zhou, Y.Y. Zhang, J.Y. Wang, X. Liang, X.H. Ma, C.H. Chen, *Electrochim. Acta 167 (2015) 25-31.*
121. R. Wu, G. Xia, S. Shen, F. Zhu, F. Jiang, J. Zhang, *Electrochim. Acta 153 (2015) 334-342.*

122. H. Liu, F. Zhang, W. Li, X. Zhang, C.S. Lee, W. Wang, Y. Tang, *Electrochim. Acta 167 (2015) 132-138.*
123. K.H. Park, D. Lee, J. Kim, J. Song, Y.M. Lee, H.T. Kim, J.K. Park, *Nano Lett., 14 (2014) 4306-4313.*
124. C. Liu, H. Huang, G.Z. Cao, F.H. Xue, R.A.P. Camacho, X.L. Dong, *Electrochim. Acta 144 (2014) 376-382.*
125. C. Zhao, L. Liu, Q. Zhang, J. Roger, H. Zhao, Y. Li, *Electrochim. Acta 155 (2015) 288-296.*
126. M. Li, J. Gu, X. Feng, H. He, C. Zeng, *Electrochim. Acta 164 (2015) 163-170.*
127. L. Zhang, S. Wang, L.X. Ding, Z. Li, H. Wang, *Electrochim. Acta 135 (2014) 35-41.*
128. D. Chen, Q. Yu, X. Xiang, M. Chen, Z. Chen, S. Song, L. Xiong, Y. Liao, L. Xing, W. Li, *Electrochim. Acta 154 (2015) 83-93.*